CHAPTER V

MULTIPLE MELTING BEHAVIOR IN ISOTHERMALLY CRYSTALLIZED POLY(TRIMETHYLENE TEREPHTHALATE)

Phornphon Srimoaon, Nujalee Dangseeyun, and Pitt Supaphol*

The Petroleum and Petrochemical college, Chulalongkorn University, Soi Chula 12, Phyathai Road, Pathumwan, Bangkok 10330, THAILAND

ABSTRACT

Melting behavior of poly(trimethylene terephthalate) (PTT) after isothermal crystallization from the melt state was studied using differential scanning calorimetry (DSC) and wide angle X-ray diffraction (WAXD) techniques. The subsequent melting thermograms for PTT isothermally crystallized within the temperature range of 182 to 215°C exhibited triple (for crystallization temperatures lower than ca. 192°C), double (for crystallization temperatures greater than ca. 192°C but lower than ca. 210°C), or single (for crystallization temperatures greater than ca. 210°C) endothermic melting phenomenon. These peaks were denoted peaks I, II, and III for low-, middle-, and high-temperature melting endotherms, respectively. For the triple melting phenomenon, it was postulated that the occurrence of peak I was a result of the melting of the primary crystallites, peak II was a result of the melting of recrystallized crystallites, and peak III was a result of the melting of the recrystallized crystallites of different stabilities. In addition, determination of the equilibrium melting temperature $T_m°$ for this PTT resin according to the linear and non-linear Hoffmann–Weeks extrapolation provided values of 243.6 and 277.6°C, respectively.

(**Key-words**: poly(trimethylene terephthalate); multiple melting behavior)

* To whom correspondence should be addressed: Fax: +662215-4459; E-mail address:pitt.s@chula.ac.th

1. INTRODUCTION

In 1941, a new type of linear aromatic polyester, poly(trimethylene terephthalate) (PTT), was successfully synthesized by Whinfield and Dickson [1], but it was not commercially available then due to the high production cost of 1,3-propanediol, a raw material used to produce PTT. With a breakthrough in the synthesis of 1,3-propanediol at a much lower cost, PTT is now commercially available and has been produced by Shell Chemicals under the tradename Corterra^{TM}. PTT has properties in between those of poly(ethylene terephthalate) (PET) and poly(buthylene terephthalate) (PBT), with an unusual combination of the outstanding properties of PET and processing characteristics of PBT. These make PTT highly suitable for uses in fiber, film and engineering thermoplastic applications.

Recently, our group reported isothermal bulk crystallization and subsequent melting behavior in PTT using differential scanning calorimetry (DSC) and wide-angle X-ray diffraction (WAXD) techniques [2]. It was found that the subsequent DSC thermograms exhibited either two or three distinct melting endotherms, depending on the temperature at which the samples were crystallized. Under the conditions studied [2], the triple melting behavior of PTT was preliminarily postulated to be a result of the melting of the primary crystallites, the melting of the recrystallized crystallites, and the melting of the recrystallized crystallites of different stabilities. Although the aforementioned postulation was satisfactory in describing our previous results, further investigation is necessary to gain a more complete understanding of the subsequent melting behavior, as well as the origin of the multiple melting behavior, in isothermally crystallized PTT.

Multiple melting is not an exclusive phenomenon for PTT. A number of investigators reported similar observations on a number of semicrystalline polymers, including some flexible polymers: polyethylene [3,4], isotactic polypropylene (i-PP) [5,6], syndiotactic polypropylene (s-PP) [7], *trans*-1,4-polyisoprene [8], and poly(butylene succinate) [9], and some semi-stiff polymers: aliphatic polyamides [10], isotactic polystyrene (i-PS) [11], syndiotactic polystyrene and its blends [12], poly(ethylene terephthalate) [13-15], poly(butylene terephthalate) [16-18], poly(phenylene sulfide) [19], and poly(aryl ether ether ketones) [20,21].

A number of hypotheses were proposed to explain the phenomenon. In the studies of isothermal crystallization of semi-crystalline polymers under quiescent conditions (i.e., crystallization is only a function of temperature), the multiple melting behavior for these polymers may be designated as being the result of one of the following reasons: the presence of two (or more) crystal modifications [5,8], the presence of two (or more) crystalline morphologies [16], the presence of two populations of crystal lamellae of different stabilities [22-25], and the simultaneous melting, recrystallization, and remelting of the lamellae initially formed at the crystallization conditions [13,26-28]. Among these models, the simultaneous melting–recrystallization–remelting and the dual-lamellar population models seem to have received much attention in explaining the multiple melting behavior in various semicrystalline polymers that do not exhibit multiple crystal modifications upon crystallizing at the crystallization conditions studied.

The simultaneous melting–recrystallization–remelting model [13,26-28] hypothesizes that the primary lamellae formed at the crystallization temperature T_c undergo a partial melting process that gives rise to an observation of the low-melting endotherm (usually observed at ca. 10°C above the T_c). During the heating scan, the partially melted material undergoes a simultaneous process of recrystallization into thicker and more perfect lamellae that, upon melting, give rise to the observation of the high-melting endotherm. This postulated model was primarily based on the observation that the magnitude and position of the low endotherm is heating rate dependent. The suitability of the model was questioned by the experimental findings that the occurrence of the high-melting endotherm precedes that of the low temperature endotherm [23,29,30], which clearly contradicts the assignment of the low endotherm to the partial melting of the primary lamellae as postulated in this model.

The dual-lamellar population model [22-25] hypothesizes that a bimodal distribution of lamellae of different stabilities exists within crystalline aggregates formed at the crystallization conditions studied, and the melting of the thin and the thick lamellae gives rise to the appearance of the low- and high-temperature endotherms, respectively. The two varients of this model [31] are the dual-lamellar stack model [21,24,30,32] and the lamellar insertion model [25]. According to the

dual-lamellar stack model, the distribution of the stacks of thick and thin lamellae is such that they exist in different stacks, while, in the lamellar insertion model, they coexist in the same stacks with the thin lamellae distributing between two thick lamellae. The applicability of these two variants in describing the experimental data is controversial and is very dependent on the experimental conditions and, perhaps, on the technique used to obtain the data.

Chung *et al.* [33] and Wu and Woo [34,35] reported the multiple melting phenomenon for isothermally crystallized PTT, similar to what has been found in this work. Chung *et al.* [33], however, attributed the occurrence of peak I to the recrystallization during the reheating scan in DSC and peaks II and III to the melting of the primary crystallites of different stabilities. On the contrary to Chung et al. [33], Wu and Woo [34] designated the occurrence of peak I to the melting of the primary crystallites. Very recently, Wu and Woo [35] suggested that the multiple melting phenomenon in PTT correlated with the ringed spherulites being formed at different T_c's. They reported that, for PTT samples exhibiting ringed spherulites (i.e., isothermally crystallized at T_c's ranging from 150 to 215°C), either double or triple endothermic peaks was observed, while, for PTT samples exhibiting non-ringed spherulites (i.e., isothermally crystallized at T_c's greater than 220°C), only single endothermic peak was observed.

Two different extrapolative methods have been used to arrive at an estimate of the equilibrium melting temperature $T_m°$ of PTT. The linear Hoffman-Weeks extrapolation (LHW) was used to obtain the $T_m°$ value of PTT as being ca. 237 [36], 244 [37], 245 [34], 248 [38], and 252°C [33], while the non-linear Hoffman-Weeks extrapolation (NLHW) arrived at the $T_m°$ value of ca. 273°C [34].

In the present contribution, differential scanning calorimetry (DSC) and wide-angle X-ray diffraction (WAXD) techniques were used to investigate the multiple melting behavior of PTT after quiescent isothermal crystallization at various temperatures, ranging from 182 to 215°C. The equilibrium melting temperature $T_m°$ of this particular PTT resin was also estimated based on the linear and non-linear Hoffman-Weeks extrapolative methods.

3. EXPERIMENTAL

3.1. Material

Poly(trimethylene terephthalate) (PTT) was supplied in pellet form by Shell Chemicals (USA) (Corterra CP509201). The weight- and number-average molecular weights for this resin were determined by size-exclusion chromatography (SEC) technique by Dr. Hoe H. Chuah and his colleagues of Shell Chemicals (USA) to be ca. 78,100 and 34,700 Daltons, respectively.

3.2. Sample Preparation

PTT resin was dried in a vacuum oven at 140°C for 5 hours prior to further use. A film of approximately 200 μm in thickness was melted-pressed at 260°C in a compression molding machine (Wabash, V50H) under an applied pressure of 4.62×10^2 MN·m^{-2}. After 5 min holding time, the film was taken out and allowed to cool at the ambient condition down to room temperature between two metal platens. This treatment assumes that previous thermo-mechanical history was essentially erased, and provided a standard crystalline memory condition for the as-prepared film.

3.3. Differential Scanning Calorimetry Measurements

A DSC (Perkin-Elmer, DSC-7) was used to investigate the multiple melting behavior of PTT. Calibration for the temperature scale was carried out using a pure indium standard (T_m^o = 156.6°C and ΔH_f^o = 28.5 J·g^{-1}) on every other run to ensure accuracy and reliability of the data obtained. To minimize thermal lag between polymer sample and the DSC furnace, each sample holder was loaded with a disc-shape sample weighing around 8.0 ± 0.3 mg which was cut from the as-prepared film. It is worth noting that each sample was used only once and all the runs were carried out under nitrogen atmosphere to prevent extensive thermal degradation.

The experiment started with heating each sample from 40°C at a heating rate of 80°C min^{-1} to a desired fusion temperature T_f of 260°C for a holding period of 5 min. After this period, each sample was rapidly cooled (i.e., at a cooling of ca. 200°C min^{-1}) from T_f to a desired crystallization temperature ranging from 182 to

215°C, where it was held until crystallization process was considered complete (when no significant change in the heat flow as a function of time was further observed). All of the subsequent melting endotherms, after isothermal crystallization at different temperatures, were recorded for further analysis.

3.4. Crystal Structure and Crystallinity Measurements

Wide-angle X-ray diffraction (WAXD) technique was used to determine the crystal modification of PTT samples prepared in the same conditions set forth for samples prepared for the DSC measurements (viz. after the samples were completely crystallized at a desired crystallization temperature, they were immediately quenched, without subsequent heating, to 30°C). Each sample was then taken out of the DSC sample holder and was pasted onto a glass X-ray sample holder, using vasaline as adhesive. The WAXD intensity pattern for each sample was then collected on an X-ray diffractometer (Rigaku, Rint 2000), equipped with a computerized data collection and analytical tools. The X-ray source (CuKα radiation, λ = 1.54 Å) was generated with an applied voltage of 40 kV and a filament current of 30 mA.

4. RESULTS AND DISCUSSION

4.1 Dependence of Subsequent Melting Endotherms on Crystallization Temperature

Figure 1 illustrates subsequent melting endotherms (10°C min^{-1}) for PTT samples isothermally melt-crystallized at various crystallization temperatures T_c ranging from 182 to 215°C. Each sample was held at 260°C for 5 min to ensure complete melting and was later quenched to the desired T_c at the highest achievable cooling rate allowed by the DSC. The total crystallization time required for completion of crystallization at each T_c varied and was found to be an increasing function of it (e.g., ca. 2 min at T_c of 182°C and ca. 8 min at T_c of 198°C). An earlier report provides a complete discussion of the bulk crystallization kinetics for this PTT resin [2].

According to Figure 1, the subsequent melting thermograms illustrated exhibited triple (for T_c's lower than ca. 192°C), double (for T_c's greater than ca.

192°C but lower than ca. 210°C), or single (for T_c's greater than ca. 210°C) endothermic melting phenomenon. These endothermic peaks were labeled as I, II, and III for low-, middle-, and high-temperature melting endotherms, respectively. The peak temperature for these endotherms was therefore denoted as the low-melting peak temperature T_I, the middle-melting peak temperature T_{II}, and the high-melting peak temperature T_{III}, respectively. Quantitative information for all of the subsequent melting thermograms recorded is summarized in Table 1.

According to Table 1, peak I was only observed for samples isothermally crystallized at T_c's greater than ca. 188°C, peak II was only observed for samples isothermally crystallized at T_c's lower than ca. 210°C, and peak III was only observed for samples isothermally crystallized at T_c's lower than ca. 192°C. Even though the positions of both peaks I and II steadily increased with increasing T_c, the variation in the position of peak II, in comparison with that of peak I, with T_c was much less obvious. Unlike peaks I and II, changes in T_c did not affect the position of peak III at all. Apart from the position of these peaks with respect to the choice of T_c used to crystallize the sample, the enthalpic information, also listed in Table 1, suggests that peak I became more pronounced, while peak II became less pronounced, with increasing T_c and that peak III was not affected by changes in T_c at all.

Before going further, we must first investigate whether the multiple melting behavior observed in PTT (within the T_c range studied) was a result of the melting of crystals of different modifications. Figure 2 shows WAXD patterns for PTT samples isothermally crystallized at T_c's ranging from 182 to 215°C. Qualitatively, all of the WAXD patterns exhibited seven characteristic peaks at the scattering angles 2θ of ca. 15.3, 16.8, 19.4, 21.8, 23.6, 24.6 and 27.3°, corresponding to the reflection planes of $(010),(0\bar{1}2),(012),(10\bar{2}),(102),(1\bar{1}3),(10\bar{4})$, respectively [39]. Since the positions of these characteristic peaks were not affected by the choice of T_c used, it is apparent that, within the T_c range studied, PTT crystallized in only one crystal modification (i.e., a triclinic unit cell with axes a = 4.64 Å, b = 6.27 Å and c = 18.64 Å, angels α = 98°, β = 90°, and γ = 112°, and space group $P\bar{1}$ [40]). Evidently, the hypothesis of

multiple crystal modifications as the source for the multiple melting behavior observed in PTT can be ruled out completely.

In s-PP, the triple melting endotherms were also observed in samples crystallized at "low" temperature [7]. The minor endotherm, located closed to each corresponding T_c, was postulated to be the melting of the secondary crystallites formed at that T_c. The low-temperature melting peak was found to be the melting of the primary crystallites formed at T_c, and the high-temperature melting peak was a result of the melting of the crystallites recrystallized during a heating scan. The triple-melting behavior observed in s-PP was therefore ascribed as contributions from melting of the secondary crystallites and their recrystallization, partial melting of the less stable fraction of the primary crystallites and their recrystallization, melting of the primary crystallites, and remelting of the recrystallized crystallites formed during the heating scan.

Based on the knowledge obtained for s-PP, preliminary postulation on the origin of the multiple melting behavior for PTT can now be offered. In PTT, the occurrence of the minor endotherm, characterizing the melting of secondary crystallites, was not so apparent, even though trace amount of such a peak was observed in the subsequent melting endotherms of samples isothermally crystallized at T_c's lower than 190°C. The occurrence of peak I was quite obvious due to the fact that it became more pronounced and shifted towards a higher temperature with increasing T_c, suggesting that peak I was likely a result of the melting of the primary crystallites. On the contrary, peak II became less pronounced and its position was not shifted so much with increasing T_c, suggesting that peak II might be only a result of the melting of the recrystallized crystallites during a heating scan. The occurrence of peak III was much less obvious, but it is logical at this point to postulate that peak III was a result of the melting of the recrystallized crystallites of different stabilities which might become prevalent at T_c's lower than 192°C. Further investigation proceeds in subsequent sub-sections.

4.2. Dependence of Subsequent Melting Endotherms on Crystallization Time Interval

It is a known fact that secondary crystallization is a very slow process and often lags behind primary crystallization. If the minor endotherm observed in subsequent melting scans of PTT was indeed attributed to the melting of the secondary crystals, one would expect that it should not be present in subsequent melting endotherms recorded at early stages of crystallization (i.e., partial crystallization for short time intervals at a given T_c). In order to test the validity of the hypothesis, separate experiments were carried out. In these experiments, PTT samples were partially crystallized for different time intervals at 182, 198, and 208°C, respectively.

Figure 3 illustrates some representative DSC melting thermograms of PTT (recorded at 20°C·min^{-1}) after isothermal crystallization at 182°C for 0.5, 0.6, 0.7, 0.8, and 1.0 min. Figure 4 shows some representative DSC melting thermograms of PTT (recorded at 20°C·min^{-1}) after isothermal crystallization at 198°C for 2.5, 3.2, 4.5, 5.5, and 7.0 min. Figure 5 exhibits some representative DSC melting thermograms of PTT (recorded at 20°C·min^{-1}) after isothermal crystallization at 208°C for 10.0, 12.5, 17.0, and 22.0 min. In addition, the quantitative description of the melting endotherms shown in Figures 6 to 8 are summarized in Table 2. At 182°C, a time interval of at least 0.3 min was required for a melting peak to be observed in the subsequent melting endotherm (not shown), while there were at least 0.5 and 1.5 min in the case of crystallization at 198 and 208°C, respectively. As a first approximation, the time intervals of ca. 0.3, 0.5, and 1.5 min corresponded to the induction time needed for stable crystallites to be formed at the respective T_c's.

A through examination of these melting endotherms suggested that the occurrence of the secondary crystallization can be decisively determined. At 182°C, the minor endotherm, located close to the T_c, was discernible after partial crystallization for at least 0.8 min, while, at 198°C, the presence of the minor endothermic shoulders was clearly visible after partial crystallization for at least 4.5 min. At 208°C, the minor endothermic shoulders were apparent on all of the subsequent melting endotherms observed. According to the data obtained for partial crystallization at 198 and 208°C, a general observation can be drawn in that the position where the minor endotherm was observed was located close to the T_c, where the sample was crystallized, and seemed to increase in its size and shift to a higher

temperature with increasing crystallization time interval at the respective T_c. This observation suggests that the existence of the minor endotherm correspond to a contribution form a rather slow crystallization mechanism occurring at the T_c, which is most likely a result of the secondary crystallization. At this point, it is logical to establish that the minor endotherm and the peak I were caused by the melting of the secondary and primary crystallites formed at the T_c.

In addition to their use for determining the source of the minor endotherm, Figures 3 to 5 provide us with additional information on the melting behavior of PTT. According to Figures 3 to 5, the positions of peak I, which were taken as the melting endotherm of the primary crystallites formed at the T_c, were essentially unaffected by changes in the crystallization time intervals. The average values of peak I were 216.9 ± 0.2°C for samples crystallized at 198°C and 222.7 ± 0.3°C for samples crystallized at 208°C, while the average values of peak II were 226.7 ± 0.4°C for samples crystallized at 198°C (see Table 2). According to the Gibbs–Thomson (GT) equation [41,42], a relationship exists between the observed melting temperature T_m and the lamellar thickness l_c of the crystallites:

$$T_m = T_m^\circ\left(1 - \frac{2\sigma_e}{\Delta H_f^\circ}\cdot\frac{1}{l_c}\right) \qquad (1)$$

where T_m° is the melting point of an infinitely thick crystal for the studied polymer and σ_e is the fold surface free energy. According to Equation (1), the fact that the positions of the peak I were essentially constant during the crystallization process suggests that the average thickness of the primary crystallites formed at each T_c is essentially constant throughout the crystallization process. In other words, the results suggested that the primary crystallites formed at the T_c did not thicken during the course of crystallization.

4.3. Dependence of Subsequent Melting Endotherms on Heating Rate

In previous sub-sections, the origin of the minor and the low-temperature melting endotherms (peak I) has been identified to be a result of the melting of the secondary and the primary crystallites formed at the respective T_c. Since we have preliminarily postulated that the occurrence of peaks II and III might be a result of

the melting of the recrystallized crystallites of two different stabilities, which were formed during a heating scan, the extent of the recrystallization process from the crystallizable materials due to the melting of the secondary and the primary crystallites significantly depends on the original T_c where these crystallites were formed, the chemical structure of the polymers studied, and the scanning rate used during the heating scan in the DSC. In addition, one can expect that the melting point of these recrystallized crystallites must be higher than that of the primary crystals formed at the T_c. The last hypothesis gives us confidence that the occurrence of peaks II and III is likely a result of the melting of the recrystallized crystallites formed during the heating scan.

To account for the effect of the heating rate on the multiple melting behavior of PTT, separate qualitative experiments were carried out. The results are shown in Figures 6 to 8. In these experiments, each sample was isothermally crystallized at 182, 198, or 208°C, and then its melting thermogram was recorded using three different scanning rates ranging from 5 to 20°C min^{-1}. It should be noted that before each measurement was carried out at a designated scanning rate, the DSC had been well calibrated for its temperature scale for that particular scanning rate. According to these figures, the appearance of the minor peak and peak I are more pronounced in the thermogram scanned at 20°C min^{-1}, as compared with those at lower scanning rates. In Figures 7 and 8, it is apparent that the weight fraction of peak II was found to decrease with increasing heating rate, while that of the peak I increased. This can be explained based on the fact that the extent of recrystalliztion process depends significantly on the scanning rate used during a heating scan. The higher the heating rate used, the shorter the time being available for the diffusion of the molecular segments onto the growing crystallites. The observation is in general accord with the results on the recrystallization kinetics in i-PP reported by Carfagna *et al.* [43].

The quantitative description of the melting endotherms shown in Figures 6 to 8 are summarized in Table 3. Apparently, the positions of peaks II and III slightly decrease with increasing heating rate for the T_c of 182°C, while the position of peak I slightly increase and that of peak II slightly decreased with increasing heating rate for the T_c's of 198 and 208°C. The cause for the increase in the observed value of

peak I may be as simple as a superheating effect, while that for the decrease in the observed values of peaks II and III should base on a more theoretical grounds. It has been previously stated that, as the scanning rate during a heating scan increased, less time was available for molecules to translate onto the growth front of the recrystallizing crystallites. As a result, the recrystallized crystallites formed at a high scanning rate should be less stable than those formed at a lower scanning rate, hence the lower value of the observed peak II.

Based on Figures 7 and 8 and the values of the enthalpy of fusion ΔH_f listed in Table 2, it is obvious that, for samples crystallized at 198°C, the weight of peak I increased, while that of peak II decreased, with increasing heating rate, and that, for samples crystallized at 208°C, peak II was clearly visible in the thermogram recorded at 5°C·min^{-1} and disappeared altogether in the thermogram recorded at 20°C·min^{-1}. These findings clearly verify out hypothesis that, during a heating scan, the less stable fraction of the primary crystallites melts (in addition to the melting of the secondary crystallites) and recrystallizes and upon further heating the recrystallized crystallites melts again, giving rise to the formation of peak II. In addition, according to the evidence shown in Figure 8, the melting of the recrystallized crystallites from melted primary crystallites during a heating scan should be largely responsible for the occurrence of peak II.

4.4. Determination of the Equilibrium Melting Temperature

It has been shown previously that peak I corresponded to the melting of the primary crystals formed at a specified T_c, thus, the T_I values listed in Table 1 are simply the T_m values of the crystalline aggregates formed in the samples after crystallization at the T_c. According to a theory derived by Hoffman and Weeks [44], the equilibrium melting temperature T_m° of a semi-crystalline polymer can be estimated by a linear extrapolation of the observed T_m–T_c data to the line $T_m = T_c$. Mathematically, they arrived at the following equation, the linear Hoffman–Weeks extrapolation (LHW):

$$T_m = \frac{T_c}{2\beta} + T_m^\circ\left[1 - \frac{1}{2\beta}\right] \qquad (2)$$

where β is the thickening ratio. In other words, β indicates the ratio of the thickness of the mature crystal l_c to that of the initial one l_c^*; therefore, $\beta = l_c/l_c^*$, which is supposed to always be greater than or equal to one. It should be noted that factor 2 in Equation (2) suggests that the thickness of the crystals undergoing melting is approximately double that of the initial critical thickness [45].

Figure 9 shows the plot of T_1 (i.e., the observed T_m value of the primary crystallites formed at a T_c) as a function of the T_c. It is evident that, within the T_c range of 188 to 208°C, the T_1 values exhibited a linear relationship with the T_c, while, within the T_c range of 210 to 215°C, a deviation from the linear trend was observed. Due to the significant non-linearity of the data within the T_c range of 210 to 215°C, only the T_1 values collected for the T_c's ranging from 188 to 208°C should be used to determined the $T_m°$ value based on the LHW extrapolation. According to Figure 9, the LHW extrapolation on the T_m–T_c data collected within the T_c range of 188 to 208°C provided the $T_m°$ value of ca. 243.6°C, with the β parameter being 0.83. The value of β near one guaranteed (based on the assumptions of the Hoffman–Weeks derivation) that the extrapolation is valid and gave a reliable $T_m°$ value, because the T_m values observed for different T_c values were not greatly affected by the lamellar thickening process, which was in a good agreement with our results discussed previously.

Even though, for the T_m–T_c data collected within the T_c range of 188 to 208°C, the correlation coefficient r^2 of the LHW fit was very close to one (i.e., r^2 = 0.9989), a slightly upward curvature of the data was clearly discernable. The upward curvature was more aggravated for the T_m data collected at the T_c's greater than 208°C. Table 4 summarizes the $T_m°$ values estimated from the T_m–T_c data collected within different T_c ranges. Evidently, the $T_m°$ value based on the LHW extrapolation was found to increase from ca. 243.6 to 256.0°C, with increasing number of data point collected at T_c's greater than 208°C. The $T_m°$ values estimated in this work are in the similar range to the values reported in the literature [33,34,37,38].

This upward curvature in the observed T_m–T_c data was also reported for various other polymer systems [45,46], thus raising a concern on the assumed constancy of the β parameter. In fact, Weeks [47] pointed out long ago that the

increase in the observed T_m value with increasing crystallization time may be a result of the lamellar thickening, which has a logarithmic dependence on time. This simply means that the thickening effect is much more severe at higher T_c values (as a result of a combination of high molecular mobility and a small relaxation time) where prolonged crystallization time is needed for complete crystallization.

Although the nonlinearity in the observed T_m–T_c data over a wide range of temperatures was explained to some extent by Alamo *et al.* [45], it is the recent contribution by Marand *et al.* [48] that offers a new method for determining the T_m° value based on the observed T_m–T_c data (provided that the T_m data obtained are essentially free from the thickening effect). Based on the Gibbs–Thomson equation (see Equation (1)) and the proposition of Lauritzen and Passaglia [49] on the stem length fluctuation during chain folding, Marand *et al.* [48] proposed a new mathematical derivation that states a relationship between the observed T_m and the corresponding T_c. This equation is called the nonlinear Hoffman–Weeks extrapolation (NLHW), which is written in the form:

$$\frac{T_m^\circ}{T_m^\circ - T_m} = \beta^m \frac{\sigma_e^1}{\sigma_e^{GT}} \frac{T_m^\circ}{T_m^\circ - T_c} + \frac{D_2 \Delta H_f^\circ}{2\sigma_e^1} \tag{3}$$

or in a simpler form:

$$M = \beta^m \frac{\sigma_e^1}{\sigma_e^{GT}} (X + a) \tag{4}$$

where β^m is the thickening coefficient (equivalent to the β parameter), σ_e^{GT} is the fold surface free energy associated with a nucleus of critical size including the extra lateral surface energy due to fold protrusion and the mixing entropy associated with stems of different lengths (σ_e^{GT} is the basal interfacial energy as appeared in the Gibbs-Thomson equation), σ_e^1 is the interfacial energy associated with the basal plane of the mature crystallite, D_2 is a constant, and all other parameters are the same as previously defined. It is worth noting that, for most cases, it is safe to assume that $\sigma_e^1 = \sigma_e^{GT}$ [48].

In order to apply Equation (3) to analyze the experimental T_m–T_c data in real polymer systems, it is required that the observed T_m data be collected from samples crystallized at different temperatures but having the same lamellar thickening

coefficient β^m. For each set of the observed T_m–T_c data, corresponding values of M and X appearing in Equation (3) can be calculated for a given choice of the seeded $T_m°$ value. In the case where $\sigma_e^1 = \sigma_e^{GT}$, the "actual" equilibrium melting temperature $T_m°$ is taken as the seeded $T_m°$ value which results in the plot of M versus X being a straight line with the slope of unity (i.e. $\beta^m = 1$) and the intercept of a (i.e. $a = D_2\Delta H_f^0/2\sigma_e^1$).

Because it has been shown previously that lamellar thickening did not occur in PTT during crystallization, at least within the T_c range studied, it is reasonable to assume that the observed T_m data summarized in Table I were collected from lamellae having the same β^m, thus making them eligible to be analyzed according to the NLHW method. Figure 10 shows variation of the M versus X, which was calculated from the data shown in Table 1 for different choices of the seeded $T_m°$ value (only the T_m–T_c data collected within the T_c range of 188 to 208°C were included in this figure). Figure 11 shows the variation in the slope of the plots of M versus X as a function of the seeded $T_m°$ value. Based on the virtue of this method, the $T_m°$ value for this PTT resin was found to be ca. 277.6°C (r^2 = 0.9980). The value of a associated with the resulting $T_m°$ value was found to be ca. 1.02. If all of the T_m data collected over the T_c range of 188 to 215°C were included in the extrapolation, the $T_m°$ value according to the NLHW extrapolation was instead found to be ca. 305.0°C (r^2 = 0.9877), and the value of a associated with this resulting $T_m°$ value was ca. 0.58. The values of the r^2 parameter obtained for fitting both sets of data suggest that NLHW extrapolation provide a better fit to the T_m–T_c data collected over the T_c range of 188 to 208°C. It should be noted that the estimated $T_m°$ value of 277.6°C agreed extremely well with the value reported by Wu and Woo [34].

5. CONCLUSIONS

Subsequent melting thermograms of PTT after isothermal crystallization at various T_c values exhibited triple (for T_c's lower than ca. 192°C), double (for T_c's greater than ca. 192°C but lower than ca. 210°C), or single (for T_c's greater than ca. 210°C) endothermic melting phenomenon. These endothermic peaks were labeled as I, II, and III for low-, middle-, and high-temperature melting endotherms,

respectively. For the triple melting phenomenon, it was postulated that the occurrence of peak I was a result of the melting of the primary crystallites formed at the T_c, peak II was a result of the melting of the recrystallized crystallites, and peak III was a result of the melting of the recrystallized crystallites of different stabilities. The formation of the recrystallized crystallites was postulated to be a result of the recrystallization of the crystallizable materials after the melting of the secondary crystallites and the partial melting of the less stable fractions of the primary crystallites formed at the T_c. The existence of peaks II and III was found to depend strongly on the stability of the secondary and the primary crystallites formed and on the scanning rate used during a heating scan. WAXD patterns confirmed that, within the T_c range of interest, PTT crystallized in a triclinic unit cell and changes in the T_c did not affect the crystal modification.

Lastly, the analysis of the observed T_m of the primary crystallites and the corresponding T_c, based on the linear and non-linear Hoffman-Weeks extrapolative methods, gave the estimated $T_m°$ values for this PTT resin of ca. 243.6 and 277.6°C, respectively.

6. ACKNOWLEDGEMENTS

The authors wish to thank Dr. Hoe H. Chuah of Shell Chemical Company (USA), Ltd. for supply of PTT and for carrying out molecular weight measurement of the supplied resin. PS acknowledges a grant provided by Chulalongkorn University through the Development Grants for New Faculty/Researchers. Partial support from the Petroleum and Petrochemical Technology Consortium and the Petroleum and Petrochemical College is also greatly acknowledged.

REFERENCES

[1] Whinfield JR and Dickson JT, Brit Pat 578,079 (June 14, 1946).

[2] Dangseeyun N, Srimoaon P, Supaphol P, and Nithitanakul M, Thermochim Acta, submitted.

[3] Alamo RG and Mandelkern L, J Polym Sci - Polym Phys 1986, 24, 2087.

[4] Freedman AM, Bassett DC, Vaughan, AS, and Olley RH, Polymer 1986, 27, 1163.

[5] Samuels RJ, J Polym Sci - Polym Phys 1975, 13, 1417.

[6] Alberola N, Fugier M, Petit D, and Fillon B, J Mater Sci 1995, 30, 1187.

[7] Supaphol P, J Appl Polym Sci 2001, 82, 1083.

[8] Lovering EG and Wooden DC, J Polym Sci A-2 1969, 7, 1639.

[9] Yoo ES and Im SS, J Polym Sci - Polym Phys 1999, 37, 1357.

[10] Liberti FN and Wunderlich B, J Polym Sci A-2 1968, 6, 833

[11] Lemstra PJ, Kooistra T, and Challa G, J Polym Sci A-2 1972, 10, 823.

[12] Woo EM and Wu FS, Macromol Chem Phys 1998, 199, 2041.

[13] Holdsworth PJ and Turner-Jones A, Polymer 1971, 12, 195.

[14] Zhou CX and Clough SB, Polym Engng Sci 1988, 28, 65.

[15] Woo EM and Ko TY, Colloid Polym Sci 1996, 274, 309.

[16] Blundell DJ, Polymer 1987, 28, 2248.

[17] Kim HG and Robertson RE, J Polym Sci - Polym Phys 1998, 36, 1757.

[18] Hsiao BS, Wang ZG, Yeh F, Gao Y, and Sheth KC Polymer 1999, 40, 3515.

[19] Cheng SZD, Wu ZQ, and Wunderlich B, Macromolecules 1987, 20, 2802.

[20] Jonas A, Russell TP, and Yoon D, Macromolecules 1995, 28, 8491.

[21] Verma RK, Marand H, and Hsiao BS, Macromolecules 1996, 29, 7767.

[22] Cebe P and Hong SD, Polymer 1986, 27, 1183.

[23] Bassett DC, Olley RH, and Raheil IAM, Polymer 1988, 29, 1745.

[24] Lattimer MP, Hobbs JK, Hill MJ, and Barham PJ, Polymer 1992, 33, 3971

[25] Kruger KN and Zachmann HG, Macromolecules 1993, 26, 5202

[26] Blundell DJ and Osborn BN, Polymer 1983, 24, 953

[27] Lee Y and Porter RS, Macromolecules 1987, 20, 1336.

[28] Lee Y, Porter RS, and Lin JS, Macromolecules 1989, 22, 1756.

[29] Cheng SZD, Cao MY, and Wunderlich B, Macromolecules 1986, 19, 1868.

[30] Verma RK, Velikov V, Kander RG, Marand H, Chu B, and Hsiao BS, Polymer 1996, 37, 5357.

[31] Verma RK and Hsiao BS, TRIP 1996, 4, 312.

[32] Hsiao BS, Wang ZG, Yeh F, Gao Y, and Sheth KC, Polymer 1999, 40, 3515.

[33] Chung WT, Yeh WJ, and Hong PD, J Appl Polym Sci 2002, 83, 2426.

[34] Wu PL and Woo EM, J Polym Sci - Polym Phys 2002, 40, 1571.

[35] Wu PL and Woo EM, J Polym Sci - Polym Phys 2003, 41, 80.

[36] Pyda M, Boller A, Grebowicz J, Chuah H, Lebedev BV, and Wunderlich B, J Polym Sci - Polym Phys 1998, 36, 2499.

[37] Kim YH, Kim KJ, and Lee KM, J Korean Fiber Soc 1997, 34, 860.

[38] Huang JM and Chang FC, J Polym Sci - Polym Phys 2000, 38, 934.

[39] Wang B, Li YC, Hanzlicek J, Cheng SZD, Gail PH, Grebowicz J, and Ho RM, Polymer 2001, 42, 7171.

[40] Desborough IJ, Hall IH, and Neisser JZ, Polymer 1979, 20, 419.

[41] Brown RG and Eby RK, J Appl Phys 1964, 35, 1156.

[42] Hoffman JD, Davis GT, and Lauritzen Jr JI. In Treatise on Solid State Chemistry; Hannay NB, Ed.; Plenum: New York, 1976; Vol. 3, Chap. 7.

[43] Carfagna C, De Rosa C, Guerra G, and Petraccone V, Polymer 1984, 25, 1462.

[44] Hoffman JD and Weeks JJ, J Res Natl Bur Stand 1962, A66, 13.

[45] Alamo RG, Viers BD, and Mandelkern L, Macromolecules 1995, 28, 3205

[46] Huang J, Prasad A, and Marand H, Polymer 1994, 35, 1896.

[47] Weeks JJ, J Res Natl Bur Stand 1963, A67, 441.

[48] Marand H, Xu J, and Srinivas S, Macromolecules 1998, 31, 8219.

[49] Lauritzen Jr JI and Passaglia E, J Res Natl Bur Stand 1967, A71, 261.

CAPTION OF TABLES

Table 1 Variation of low-melting peak temperature T_I, middle-melting peak temperature T_{II}, high-melting peak temperature T_{III}, and enthalpy of fusion ΔH_f for PTT measured at various crystallization temperatures T_c

Table 2 Variation of low-melting peak temperature T_I, middle-melting peak temperature T_{II}, and enthalpy of fusion ΔH_f for PTT measured at crystallization temperatures T_c of 182, 198, and 208°C for various crystallization time intervals

Table 3 Variation of low-melting peak temperature T_I, middle-melting peak temperature T_{II}, high-melting peak temperature T_{III}, and enthalpy of fusion ΔH_f for PTT measured at crystallization temperatures T_c of 182, 198, and 208°C for various heating rates

Table 4 Variation of estimated equilibrium melting temperature $T_m°$ according to linear Hoffman-Weeks extrapolative method for different observed melting temperature T_m – crystallization temperature T_c data ranges

CAPTIONS OF FIGURES

Figure 1 Subsequent melting endotherms (recorded at 10°C·min^{-1}) for PTT samples isothermally crystallized from the melt state at different crystallization temperatures.

Figure 2 Wide-angle X-ray diffractograms for PTT samples isothermally crystallized from the melt state.

Figure 3 Subsequent melting endotherms (recorded at 20°C·min^{-1}) for PTT samples after partial crystallization at 182°C for different time intervals.

Figure 4 Subsequent melting endotherms (recorded at 20°C·min^{-1}) for PTT samples after partial crystallization at 198°C for different time intervals.

Figure 5 Subsequent melting endotherms (recorded at 20°C·min^{-1}) for PTT samples after partial crystallization at 208°C for different time intervals.

Figure 6 Subsequent melting endotherms for PTT samples recorded using different heating rates ranging from 5 to 20°C·min^{-1} after crystallization at 182°C.

Figure 7 Subsequent melting endotherms for PTT samples recorded using different heating rates ranging from 5 to 20°C·min^{-1} after crystallization at 198°C.

Figure 8 Subsequent melting endotherms for PTT samples recorded using different heating rates ranging from 5 to 20°C·min^{-1} after crystallization at 208°C.

Figure 9 Observed melting temperature of the primary crystallites as a function of crystallization temperature for PTT shown along with the linear Hoffman–Weeks extrapolation (solid line) and the non-linear Hoffman-Weeks extrapolation.

Figure 10 Plots of the scaled observed melting temperature [$M = T_m°/(T_m° - T_m)$] versus the scaled crystallization temperature [$X = T_m°/(T_m° - T_c)$] for various choices of the seeded equilibrium melting temperature ($T_m°$) for PTT (for the data collected over the T_c range of 188 to 208°C).

Figure 11 The variation of the thickening coefficient (β^m) as a function of the seeded equilibrium melting temperature ($T_m°$) for PTT (for the data collected over the T_c range of 188 to 208°C).

Table 1 Variation of low-melting peak temperature T_I, middle-melting peak temperature T_{II}, high-melting peak temperature T_{III}, and enthalpy of fusion ΔH_f for PTT measured at various crystallization temperatures T_c

T_c °C	T_I °C	ΔH_{fI} J·g^{-1}	T_{II} °C	ΔH_{fII} J·g^{-1}	T_{III} °C	$\Delta H_{fII+III}$ J·g^{-1}	Sum of ΔH_f J·g^{-1}
182	-	-	221.8	-	227.5	56.3	56.3
184	-	-	222.0	-	227.0	53.5	53.5
186	-	-	223.3	-	226.9	54.0	54.0
188	209.9	0.80	223.8	-	226.7	54.7	55.5
190	211.2	1.19	225.5	-	227.0	51.4	52.6
192	212.4	2.58	225.4		226.5	49.5	52.1
194	213.7	4.21	225.9	46.3	-	-	50.6
196	214.9	5.97	225.9	44.4	-	-	50.4
198	216.2	7.58	226.5	41.0	-	-	48.6
200	217.4	12.3	227.0	39.0	-	-	51.3
201	218.0	13.7	227.4	35.2	-	-	48.9
202	218.5	15.7	227.7	35.9	-	-	51.6
203	219.2	16.0	227.9	31.0	-	-	47.0
204	219.7	20.9	228.0	28.5	-	-	49.4
205	220.0	25.1	227.7	25.8	-	-	50.9
206	220.7	27.6	228.2	23.9	-	-	51.5
207	221.4	35.2	227.9	16.5	-	-	51.7
208	222.2	-	227.9	-	-	-	52.8
210	224.7	-	229.4	-	-	-	59.4
211	226.0	-	-	-	-	-	62.3
212	226.7	-	-	-	-	-	59.0
213	226.9	-	-	-	-	-	59.2
215	228.9	-	-	-	-	-	56.8

Table 2 Variation of low-melting peak temperature T_I, middle-melting peak temperature T_{II}, and enthalpy of fusion ΔH_f for PTT measured at crystallization temperatures T_c of 182, 198, and 208°C for various crystallization time intervals

T_c = 182°C			T_c = 198°C					T_c = 208°C		
Time Interval	T_{II}	ΔH_{fII}	Time Interval	T_I	ΔH_{fI}	T_{II}	ΔH_{fII}	Time Interval	T_I	ΔH_{fI}
min	°C	$J \cdot g^{-1}$	min	°C	$J \cdot g^{-1}$	°C	$J \cdot g^{-1}$	min	°C	$J \cdot g^{-1}$
0.5	225.7	35.6	2.5	216.7	4.6	226.4	12.1	10.0	222.4	6.3
0.6	226.4	36.6	3.2	216.7	7.3	226.4	18.3	12.5	222.7	13.3
0.7	226.4	46.6	4.5	217.1	11.1	226.7	25.3	17.0	222.7	21.4
0.8	227.1	48.9	5.5	217.1	13.4	227.1	29.5	22.0	223.1	35.6
1.0	227.1	52.6	7.0	217.1	15.5	227.1	33.2	-	-	-

Table 3 Variation of low-melting peak temperature T_I, middle-melting peak temperature T_{II}, high-melting peak temperature T_{III}, and enthalpy of fusion ΔH_f for PTT measured at crystallization temperatures T_c of 182, 198, and 208°C for various heating rates

	T_c=182°C			T_c=198°C				T_c=208°C		
Heat Rate	T_{II}	T_{III}	ΔH_f	T_I	ΔH_{fI}	T_{II}	ΔH_{fII}	T_I	T_{II}	$\Delta H_{f\,total}$
°C·min^{-1}	°C	°C	J·g^{-1}	°C	J·g^{-1}	°C	J·g^{-1}	°C	°C	Jg^{-1}
5	221.4	228.6	57.9	215.9	4.9	226.9	44.2	221.6	229.0	50.5
10	221.1	227.5	56.3	216.2	7.6	226.5	41.0	222.2	227.8	59.9
20	-	226.7	52.9	217.1	15.1	226.1	31.6	223.1	-	56.1

Table 4 Variation of estimated equilibrium melting temperature $T_m°$ according to linear Hoffman-Weeks extrapolative method for different observed melting temperature T_m – crystallization temperature T_c data ranges

T_m–T_c °C	β	$T_m°^{LHW}$ °C	r^2
188-208	0.829	243.6	0.9989
188-210	0.802	246.1	0.9931
188-211	0.773	249.4	0.9866
188-212	0.752	252.1	0.9843
188-213	0.743	253.6	0.9855
188-215	0.728	256.0	0.9855

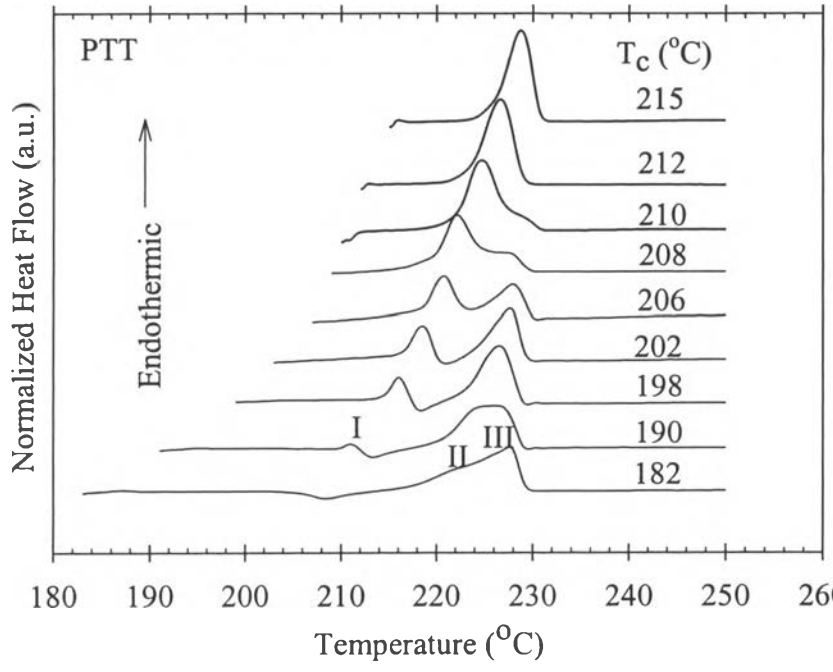
PTT
T_c (°C)
215
212
210
208
206
202
198
190
182
Endothermic
I
II
III
Normalized Heat Flow (a.u.)
180
190
200
210
220
230
240
250
260
Temperature (°C)

Figure 1

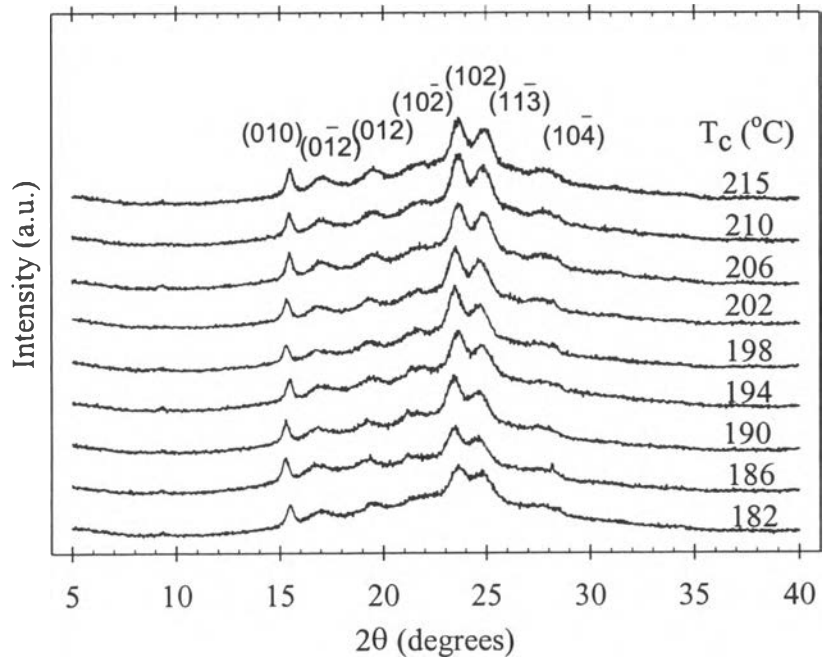
(010)
(01$\bar{2}$)
(012)
(10$\bar{2}$)
(102)
(11$\bar{3}$)
(10$\bar{4}$)
T_c (°C)
215
210
206
202
198
194
190
186
182
Intensity (a.u.)
5
10
15
20
25
30
35
40
2θ (degrees)

Figure 2

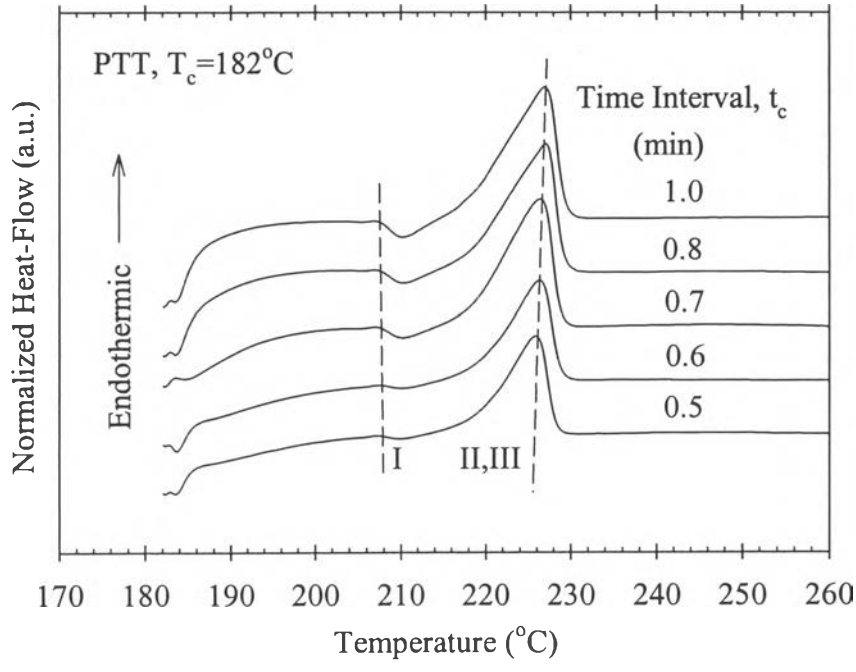
PTT, T_c=182°C
Time Interval, t_c
(min)
1.0
0.8
0.7
0.6
0.5
Endothermic
I
II,III
Normalized Heat-Flow (a.u.)
170
180
190
200
210
220
230
240
250
260
Temperature (°C)

Figure 3

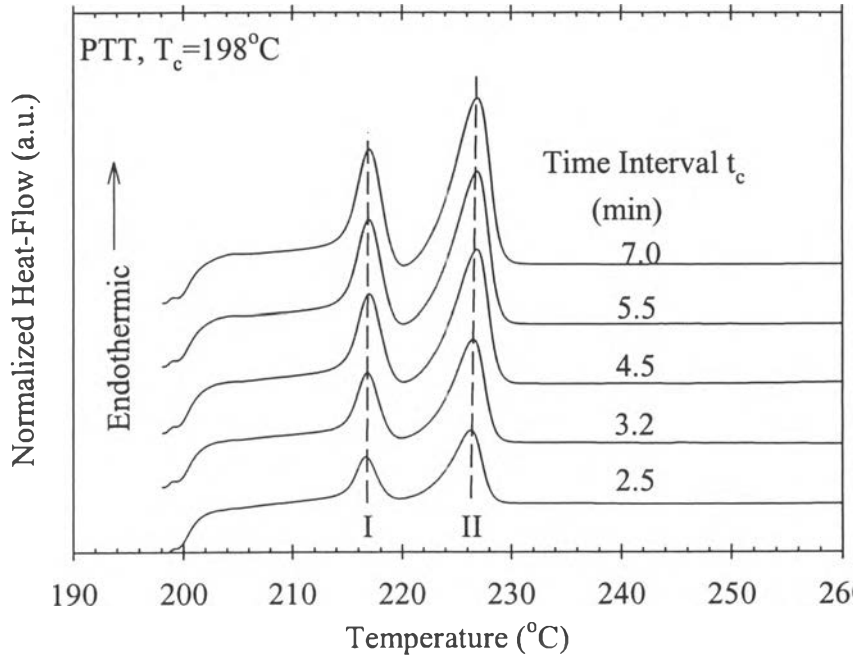
PTT, T_c=198°C
Time Interval t_c
(min)
7.0
5.5
4.5
3.2
2.5
Endothermic
I
II
Normalized Heat-Flow (a.u.)
190
200
210
220
230
240
250
260
Temperature (°C)

Figure 4

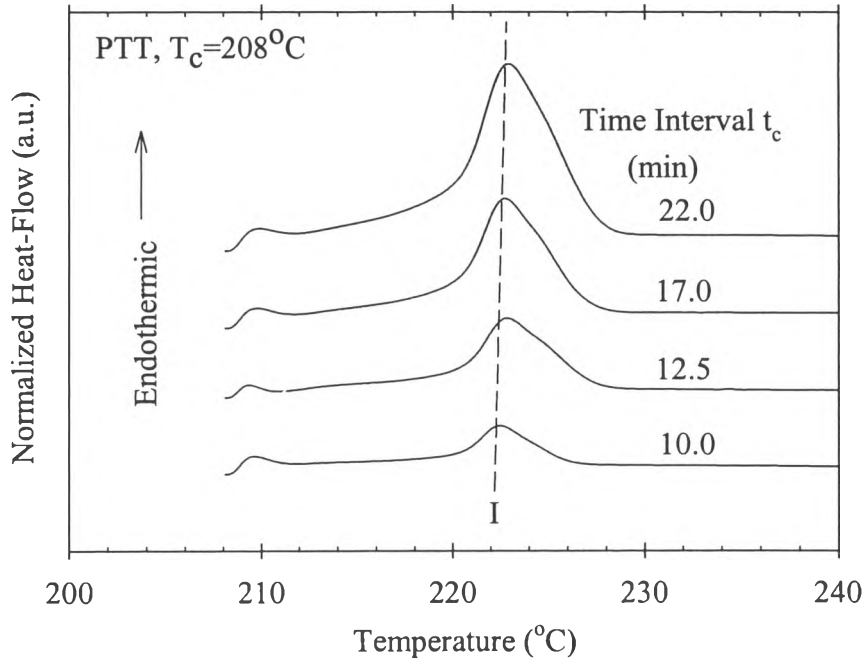
PTT, T_c=208°C
Time Interval t_c
(min)
22.0
17.0
12.5
10.0
Endothermic
I
Normalized Heat-Flow (a.u.)
200
210
220
230
240
Temperature (°C)

Figure 5

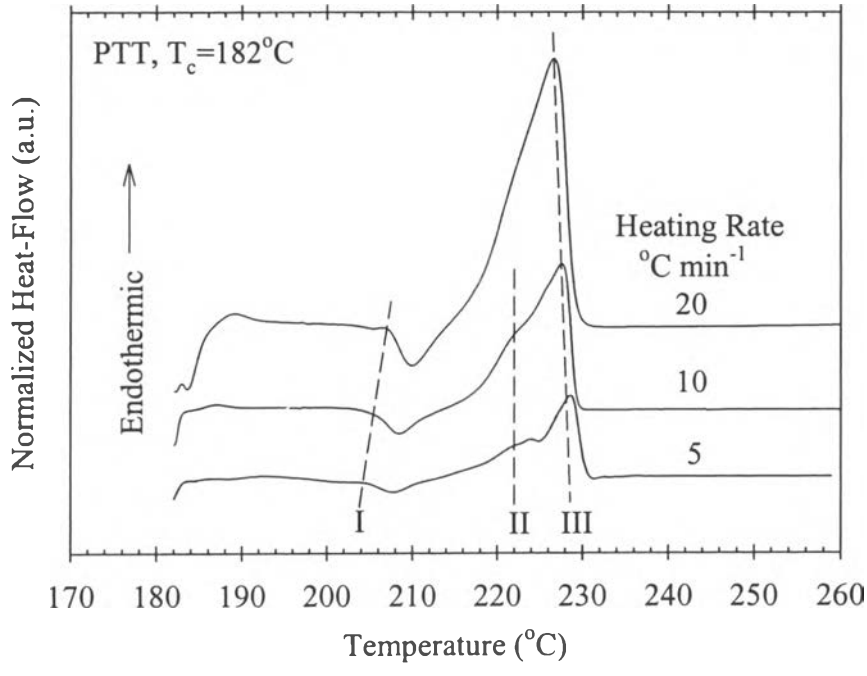
PTT, T_c=182°C
Endothermic
Normalized Heat-Flow (a.u.)
Heating Rate
°C min^{-1}
20
10
5
I
II
III
170
180
190
200
210
220
230
240
250
260
Temperature (°C)

Figure 6

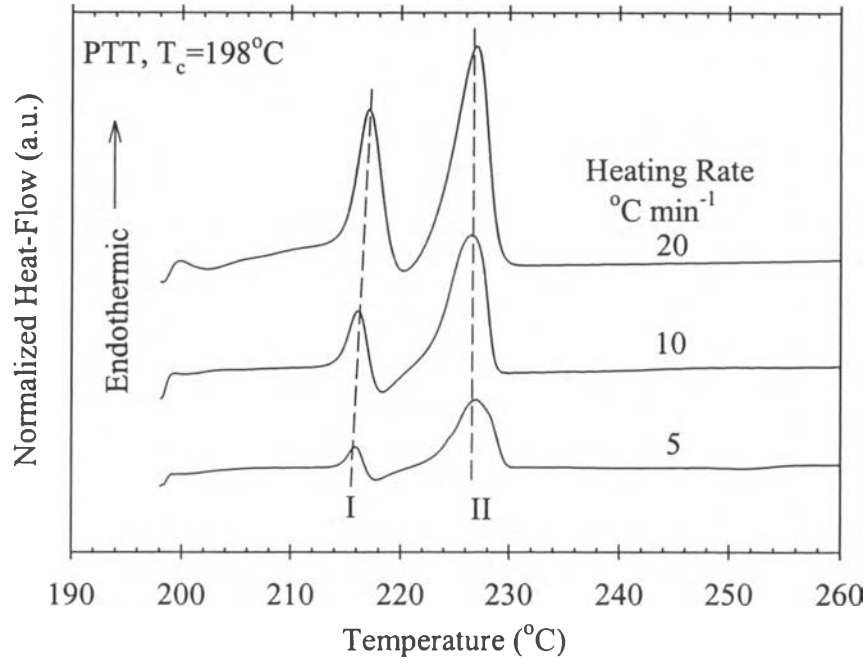
PTT, T_c=198°C
Endothermic
Heating Rate
°C min^{-1}
20
10
5
I
II
Normalized Heat-Flow (a.u.)
190
200
210
220
230
240
250
260
Temperature (°C)

Figure 7

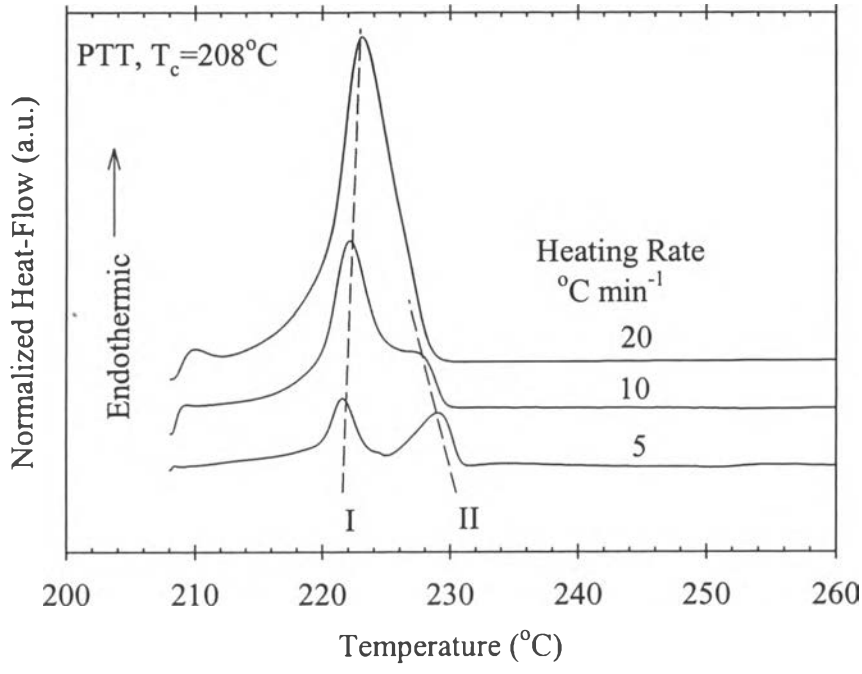
PTT, T_c=208°C
Endothermic
Normalized Heat-Flow (a.u.)
Heating Rate
°C min^{-1}
20
10
5
I
II
200
210
220
230
240
250
260
Temperature (°C)

Figure 8

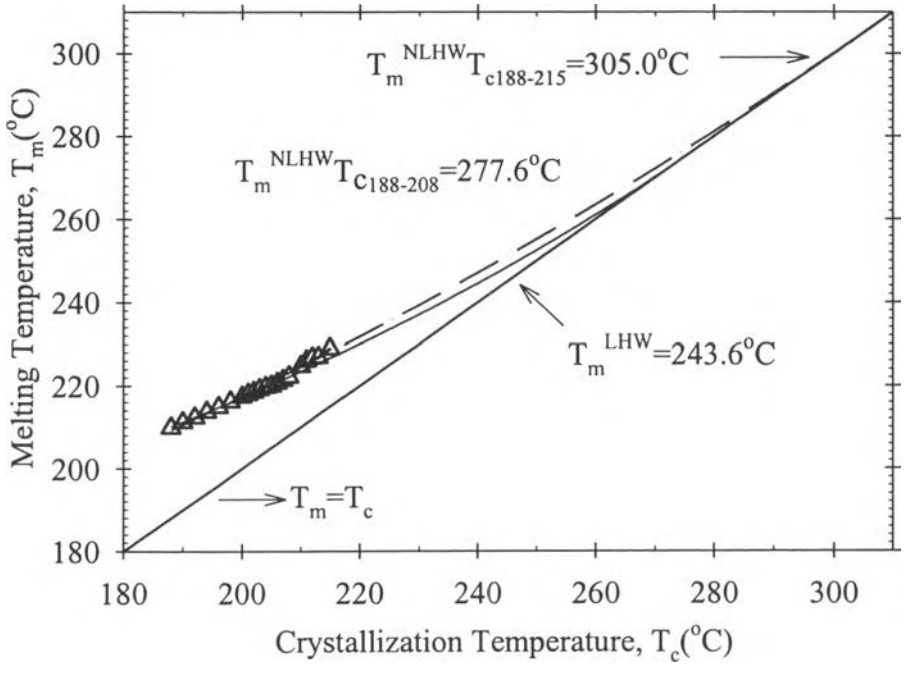
$T_m^{NLHW}T_{c188-215}$=305.0°C
$T_m^{NLHW}T_{c188-208}$=277.6°C
T_m^{LHW}=243.6°C
T_m=T_c
Melting Temperature, T_m(°C)
Crystallization Temperature, T_c(°C)
180
200
220
240
260
280
300

Figure 9

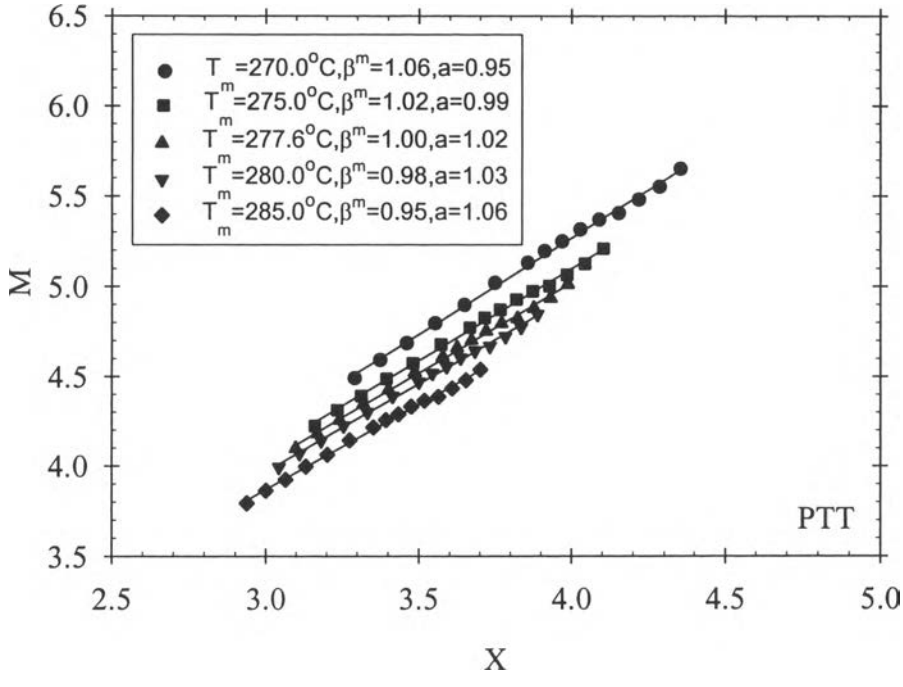
T_m=270.0°C,β^m=1.06,a=0.95
T_m=275.0°C,β^m=1.02,a=0.99
T_m=277.6°C,β^m=1.00,a=1.02
T_m=280.0°C,β^m=0.98,a=1.03
T_m=285.0°C,β^m=0.95,a=1.06
PTT
M
X
6.5
6.0
5.5
5.0
4.5
4.0
3.5
2.5
3.0
3.5
4.0
4.5
5.0

Figure 10

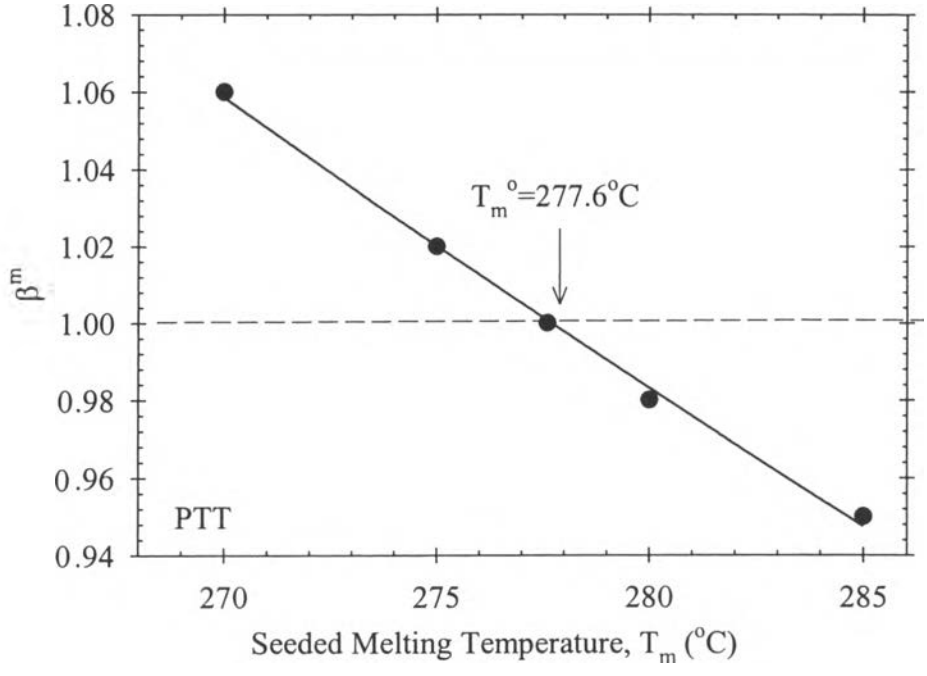
1.08
1.06
1.04
1.02
1.00
0.98
0.96
0.94
β^m
T_m^o=277.6°C
PTT
270
275
280
285
Seeded Melting Temperature, T_m (°C)

Figure 11